Published in final edited form as:
Dent Mater. 2009 October ; 25(10): 1195–1204. doi:10.1016/j.dental.2009.04.005.

Structure, chemical composition and mechanical properties of coronal cementum in human deciduous molars

Sunita P. Ho[1], **Pavla Senkyrikova**[1], **Grayson W. Marshall**[1], **Wenbing Yun**[2], **Yong Wang**[3], **Kunal Karan**[3], **Cheng Li**[4], and **Sally J. Marshall**[1]

[1]Division of Biomaterials and Bioengineering, Department of Preventive and Restorative Dental Sciences, UCSF, CA 94143-0758

[2]Xradia Inc., 5052 Commercial Circle, Concord, CA, USA 94520

[3]Department of Oral Biology, University of Missouri Kansas City, USA

[4]Department of Bioengineering, UC Berkeley, CA 94720-1762

Abstract

Objectives—It was hypothesized that the coronal cementum containing collagen forms a weak junction with enamel unlike the well integrated DEJ and CDJ.

Methods—The hypothesis was investigated in two parts: 1) Evaluate the structure, chemical composition and mechanical properties of coronal cementum and its junction with enamel using scanning electron microscopy, micro-X-ray computed tomography, and atomic force microscopy. The chemical composition and mechanical properties were determined by evaluating the spatial variations of inorganic (PO_4^{3-} ν_1 mode at 960 cm^{-1}) and organic (C-H deformation at 1452 cm^{-1}; C-H stretch at 2940 cm^{-1}) contents using Raman microspectroscopy and elastic modulus and hardness values using nanoindentation. 2). Estimate the strength and evaluate the microstructure of coronal cementum interface with enamel using SEM and MicroXCT™.

Results & Conclusions—Coronal cementum is heterogeneous because it is a combination of laminar acellular afibrillar cementum and acellular extrinsic fiber cementum with relatively higher organic content. It integrates micromechanically via a scallop-like weak interface with enamel unlike the biomechanically efficient DEJ and CDJ and is continuous with primary root cementum. A single tooth could exhibit all three types of cementum enamel junctions; an overlap, butt and a gap depending on the sectioning plane. The elastic modulus of coronal cementum (11.0 ± 5.8 GPa) is significantly lower ($p < 0.05$; Student's t-test with 95% confidence interval) than primary cementum (15.8 ± 5.3 GPa).

Keywords

coronal cementum; atomic force microscopy; interface; structure; chemical composition; mechanical properties; cementum enamel junction

INTRODUCTION

The load bearing mineralized tissues of a tooth are well integrated by biomechanically efficient interfaces that include dentin enamel junction (DEJ) in the crown and cementum dentin junction (CDJ) in the root [1-4]. There is a third interface in the coronal portion of the tooth called the cementum enamel junction (CEJ). Traditionally three types of CEJ have been reported. These include: 1) overlap; in which cementum overlaps enamel and is called coronal cementum (CC) 2) abutment; cementum butts with enamel and 3) gap; a finite space between

cementum and enamel, exposing cervical dentin. Although controversial, of the three types, the overlap CEJ was reported to occur most frequently in human teeth [5,6].

Cementum is an essential mineralized dental tissue and is a part of the attachment apparatus within the periodontium. Functionally, in the root, it is responsible for cementing the principal collagen fibers of the periodontal ligament [7] thus attaching the tooth to the alveolar bone. From a materials perspective, root cementum is inhomogeneous owing to its varying structure and chemical composition resulting in a range of elastic modulus values [8-10]. Although little is known about the physical properties and function of coronal cementum, anatomically, coronal cementum forms a junction with enamel in most mammalian species [11].

In this study it was hypothesized that the coronal cementum containing collagen forms a weak junction with enamel unlike the well integrated DEJ and CDJ. To investigate the hypothesis the study was divided in two objectives: 1) Evaluate the structure, chemical composition and mechanical properties of coronal cementum and its junction with enamel using scanning electron microscopy, micro-X-ray computed tomography, and atomic force microscopy. The chemical composition and mechanical properties were determined by evaluating the spatial variations of inorganic (PO_4^{3-} ν_1 mode at 960 cm^{-1}) and organic (C-H deformation at 1452 cm^{-1}; C-H stretch at 2940 cm^{-1}) contents using Raman microspectroscopy and elastic modulus and hardness values using nanoindentation. 2). Estimate the strength and evaluate the microstructure of coronal cementum interface with enamel using SEM and MicroXCT™.

2. MATERIALS AND METHODS

2.1. Specimen preparation for AFM, AFM-based nanoindentation and Raman microspectroscopy

Several human deciduous mandibular molars were collected following a protocol approved by the UCSF Committee on Human Research, sterilized and stored in Hank's balanced salt solution (HBSS) [12]. The teeth are routinely sterilized using 0.31 Mrad of γ-radiation [12]. Twenty teeth (N=20) (10% of the total population of teeth collected) with cementum predominantly overlapping enamel were selected based on light microscopy study.

The teeth were longitudinally sectioned in half with the use of a diamond-wafering blade and a low-speed saw (Isomet, Buehler Ltd., Lake Bluff, IL) under wet conditions. The specimens were embedded in epoxy resin (Stycast, Emerson & Cuming, Billerica, MA). Embedding of specimens facilitated retention of the native structure necessary for further physical property characterization of coronal cementum and its interface with enamel. The specimens were trimmed to 5 – 7 mm^3 to accommodate the spatial requirements of the respective specimen holders for various microscopy techniques. After trimming, the specimens were polished using a 1200 silicon carbide grit paper (Buehler, Lake Bluff, IL), followed by a series of fine polishing diamond suspension slurries: 6 μm, 3 μm, and 1 μm (Buehler, Lake Bluff, IL). The specimens were ultrasonicated in distilled water for 10 s each before proceeding to the next finer level of polishing. Subsequently they were mounted on steel stubs (Ted Pella, Inc., Redding, CA) using cyanoacrylate adhesive (MDS Adhesive QX-4, MDS Products, Inc., Anaheim, CA) for AFM characterization and using double adhesive carbon tape for SEM characterization. Prior to high-resolution characterization using an AFM and SEM, the coronal cementum for all specimens was identified using a light microscope (10x-60x, BX-51, Olympus, Tokyo, Japan) with an Image-Pro software (Image-Pro Plus Microscope, version 4.0; Media Cybernetics, Silver Spring, MD).

2.2. SEM of polished CEJ blocks

The polished specimens were placed directly into the SEM (Topcon ISI, SX40A, Pleasanton, CA) observed under environmental conditions (100mTorr) C-FAS (charge free anti-contamination system) at 150x-5000x magnification. After a 30 minute interval inside the SEM the specimens were imaged again to identify possible peeling of coronal cementum.

2.3. Microstructural analysis of ground sections of CEJ using MicroXCT™

150-300 μm thick longitudinal ground sections were prepared using basic metallography polishing techniques as described above. However, 1200 grit polishing paper was not used because it was believed to damage the surface of coronal cementum and its interface with enamel. Micro-scale structural analysis of the coronal cementum integration with enamel was performed using X-ray micro-tomography (MicroXCT™) (Xradia, Inc. Concord, CA) at 20X. Computed tomography (CT) facilitates viewing an object in 3D and allows selection of virtual parallel slices spaced by 1 μm in different planes thus illustrating bulk structure of tissues. The transmission X-ray imaging of the specimens was performed using an X-ray tube with a tungsten anode setting of 40 kV at 4W.

2.4. Structure analysis of coronal cementum using an AFM

Qualitative and quantitative structure analyses of coronal cementum and CEJ was performed using a contact mode AFM under both dry and wet conditions (Nanoscope III, Multimode; DI-Veeco Instruments Inc., Santa Barbara, CA). Some specimens (N = 5) were etched using EDTA (0.5M, pH 7.4) for 10 minutes. Etching facilitated removing surface and subsurface layers of mineral revealing the basic organic constituent of extracellular matrix, i.e. collagen. The polished-only and etched specimens were scanned using a Si_3N_4 tip attached to a "V-shaped" cantilever with a nominal normal spring constant of 0.03N/m (DI-Veeco Instruments Inc., Santa Barbara, CA) at a scanning frequency of 1 Hz. The nominal radius of curvature of the tip was less than 50 nm. The various topographical features were analyzed using Nanoscope III version 4.43r8 software (Nanoscope III, Multimode; DI-Veeco Instruments, Inc., Santa Barbara, CA).

2.5. Chemical composition of coronal cementum using Raman micro-spectroscopy

The spatial distribution of organic and inorganic components was determined from the relative intensities of corresponding peaks using Raman microspectroscopy (HR800, Jobin Yvon Inc., HORIBA Group, Edison, NJ) as described previously [13]. An excitation laser with an operating wavelength of 623.8 nm was used. The relative inorganic (PO_4^{3-} ν_1 mode at 960 cm^{-1}) and organic (C-H deformation at 1452 cm^{-1}; C-H stretch at 2940 cm^{-1}) contents of coronal cementum under dry conditions were recorded by performing line and area imaging of maximum relative intensities at the respective inverse wave-numbers after subtracting the luminescence background. Raman spectra of C-H stretch at 2940 cm^{-1} from 15 points along the length of coronal cementum were collected at 20X. The data were averaged over 2 collection periods of 60 seconds for each spectrum. Raman spectra from an area of 45 μm × 45 μm with a spacing of 1.5 μm between points were collected at 50X. The data were averaged over 2 collection periods of 45 seconds for each spectrum. The ratio of the relative intensities of organic (C-H deformation at 1452 cm^{-1}) to inorganic (PO_4^{3-} ν_1 mode at 960 cm^{-1}) was taken to remove the probable influence of bulk structure within respective tissues on the acquired relative intensities of the organic and inorganic Raman signals. It should be noted that the varying packing density of enamel and cementum could influence the relative intensities of the organic and inorganic Raman signals.

2.6. Reduced elastic modulus of coronal cementum using site-specific nanoindentation

Nanomechanical tests under dry and wet conditions of coronal and primary cementum in deciduous molars were performed using a Triboindenter (Hysitron, Minneapolis, MN) with a 100 nm Berkovich diamond tip. Nanoindentation was performed dry and wet, by immersing the specimen and the indenter probe in water. The maximum normal load was 1000 μN, with load, hold, and unload for 3s each. The distance between any two indents on average was 5 μm ranging from 5 – 10 μm depending on location of the indent. Calibration was done using a fused silica standard and the reduced elastic modulus was evaluated using the Oliver-Pharr method [18].

3. RESULTS

3.1. Hierarchical length-scale structural analysis of overlap cementum using light and atomic force microscopy techniques, and MicroXCT™

It should be noted that a single tooth could contain all three types of cementum enamel junctions. However, low resolution micro-scale studies, using light microscopy facilitated identifying specimens with predominantly overlap cementum. Specimens containing either an abutment or gap cementum enamel junction were discarded because the existing cementum is primary and not coronal cementum which is of interest in this study. Figure 1a illustrates three specimens with cementum overlapping enamel as shown by the red line. Peeling of coronal cementum from enamel can also be observed in all three specimens; a common occurrence even under wet conditions, however, most frequently observed under dry conditions.

The free surface of the specimens was imaged under vacuum at a higher resolution using an SEM. A distinct peeling (Figure 1b) of coronal cementum was observed. Notice that the peeling initiated a crack which propagated through granular mantle dentin. Additionally, cracks generated mostly at the free surface of primary cementum (white arrow head in Figure 1b) often propagated along the grain of the extracellular matrix i.e. along the radial collagen fiber direction which is the characteristic structure of primary cementum (Figure 1b).

Evaluation of the 2D reconstructed slices taken through the thickness of the specimen obtained using MicroXCT™ illustrated peeling-off of coronal cementum from enamel, but also revealed an interesting localized scallop-like interdigitation of enamel pits and cementum protrusions (Figure 2). The 2D slices illustrate coronal cementum and the scalloped appearance at the interface (red arrows in Figure 2) where the enamel pits accommodate the cementum protrusions (red arrows point to the pits in Figure 2). MicroXCT™ 2D reconstructed slices illustrate the varying length of coronal cementum through the thickness of specimen (Figure 3). This is indicative that the length of cementum overlapping enamel i.e. length of coronal cementum varies around the tooth.

High resolution microscopy using an atomic force microscope of specimens treated with EDTA to reveal the collagen network, illustrated the inherent structure of coronal cementum. In Figure 4, the coronal cementum (CC) is categorized into the following regions: distal (area A1) (Figure 4a), mid (area A2) (Figure 4b), proximal (area A3) (Figure 4c) and cervical (area A4) (Figure 4d), with respect to the tooth cervix. The distal- and mid-CC illustrated narrow lamellar-like material adjacent to enamel which is denoted as acellular afibrillar cementum (AAC). Adjacent to AAC was acellular extrinsic fiber cementum (AEFC) with no lamellar pattern. However, at a higher resolution, AEFC contained several collagen fibrils (bottom figures 4a and 4b). Lamellar-like AAC was also observed in proximal-CC, however, was not identified in cervical-CC (top figures 4c and 4d). Both, proximal-CC and cervical-CC contained collagen fibrils (AEFC, bottom figures 4c and 4d).

3.2. Chemical composition of coronal cementum

Figure 5a illustrates the distribution of organic matrix represented by the presence of C-H stretch at 2940 cm^{-1} taken from three different specimens. Figure 5b illustrates the distributions of PO_4^{3-} ν_1 mode at 960 cm^{-1} (top micrograph of Figure 5b) and C-H deformation at 1452 cm^{-1} (middle micrograph of Figure 5b) which are indicative of both inorganic and organic within an area of 45 μm × 45 μm. The ratio of organic to inorganic illustrates the dominance of the organic matter in coronal cementum.

3.3. Elastic modulus and hardness of coronal cementum

The spread of raw data of elastic modulus and hardness values of coronal and primary cementum under dry and wet conditions are shown in Figure 6. The elastic modulus and hardness values of PC and CC under dry conditions were significantly higher ($p < 0.05$, Student's t-test with a confidence level of 95%) than under wet conditions. The average elastic modulus values of dry-CC (15.7 ± 8.7 GPa) and wet-CC (11.0 ± 5.8 GPa) were significantly lower than respective dry-PC (18.5 ± 7.4 GPa) and wet-PC (15.8 ± 5.3 GPa). The average hardness values of dry-CC (1.3 ± 1.7 GPa) and wet-CC (0.8 ± 1.3 GPa) were not significantly different ($p > 0.05$) from respective dry-PC (0.7 ± 0.3 GPa) and wet-CC (0.8 ± 1.3 GPa).

4. DISCUSSION

This study was performed to answer the following questions: Is coronal cementum mechanically integrated with enamel? Does coronal cementum contain organic matter? What are the physical properties of coronal cementum? These questions were investigated by characterizing the attachment of coronal cementum, its inherent structure and mechanical properties using human deciduous teeth.

Despite previous reports on common occurrence of overlap CEJ, it was a challenge to find teeth containing coronal cementum. This could be due to three reasons: 1) naturally, coronal cementum length could vary around the circumference of a crown, which can lead to several types of CEJ within a tooth depending on the sectioning plane. 2) The extraction process may induce significant damage and disrupt the coronal cementum, thus creating an artifact. 3) Because of its anatomical location, and cementum in general being a relatively softer mineralized tissue; tooth brushing, flossing and other dental hygiene related events could lead to loss of coronal cementum [15]. Hence, human deciduous molars were chosen because of their natural exfoliation characteristic in comparison to clinically extracted teeth, including the reduced chance of changes associated with periodontal or hygiene treatment.

Coronal cementum forms a weak junction with enamel via a scallop-like integration

Teeth with cementum coronal to tooth cervix were categorized as those containing an overlap CEJ. Regardless of the length of coronal cementum from tooth cervix, most often the thinner distal coronal cementum peeled away from the enamel surface (Figures 1-3).

Most often interfacial strength can be tested using different types of loads apart from traditional mechanical loads. In this study, hydrostatic pressure within tissues was modified by controlling the environmental pressure and humidity in order to estimate the interfacial strength of an overlap CEJ. This was done by placing the specimens in a specimen chamber of an SEM where both pressure and humidity are controlled to maintain proper operating conditions while performing real time imaging of the specimen. The specimens were studied under vacuum (100 mTorr) and seemingly moist conditions. Under these conditions, the differential strain due to differential shrinkage of enamel and cementum resulted in a stress concentration at the CEJ followed by a peel-off of coronal cementum classifying it as a weaker interface in comparison to the DEJ or CDJ. However, it should be noted that a differential strain of varying magnitude

also occurs at the DEJ and CDJ but due to the superior structural and chemical integration of respective tissues, delamination at these respective interfaces was not observed.

Additionally, a possible scallop-like mechanism by which coronal cementum could be integrated with enamel was observed (Figure 2). MicroXCT™ illustrated various enamel pits and cementum protrusions throughout the specimen thickness (Figure 2). This observation is similar to scallop-like cementum-enamel integration found on occlusal surfaces of herbivorous mammalian teeth [16,15,17,18].

In humans, coronal cementum is found as a thin layer adjacent to enamel in the cervical portion of the tooth and not on occlusal surfaces as mostly seen in herbivorous mammals [15]. Developmentally, the presence or absence of the reduced enamel epithelium layer during formative and eruptive phases of mammalian teeth, defines the amount of coronal cementum [19]. In most herbivores, the epithelium degenerates prior to enamel maturation generating residual pits in the enamel formative surface. The resulting surface topography provides a conducive environment for cementoblasts that eventually form coronal cementum [20]. However, in humans, the persistent epithelium layer over enamel during development and eruptive phases could explain the lack of cementum over a larger surface area of enamel [18, 19]. During development the cementoblasts and ameloblasts are in close proximity and random variations in the surface topography of enamel may lead to a coating by cementoblasts resulting in the observed integration of cementum protrusion and enamel pits. The random distribution of enamel pits and protrusions suggests the observed coronal cementum-enamel integration could be incidental to tooth development.

Soft tissue may be attached to coronal-cementum. In healthy individuals, the junctional epithelium hemidesmosomal attachment ends at or slightly coronal to the cervix [6]. Immediately apical to the end of the junctional epithelial attachment is the first source of collagen attachment via the dentogingival fiber group [21].

Coronal cementum also contains collagen

Corroborating with previous reports, AFM results illustrated two types of coronal cementum, acellular afibrillar cementum (AAC) and acellular extrinsic fiber cementum (AEFC) [11]. The AAC consists of mineralized matrix characterized by its lack of cells and collagen fibrils and the presence of laminated apposition lines [22,7,11].

Spectroscopically, point-by-point analysis within coronal cementum illustrated the presence of organic matter as indicated by C-H stretch peak at 2940 cm^{-1}. Mapping organic matter at 2940 cm^{-1} along the length of coronal cementum (Figure 5a) and the ratio of organic (C-H at 1452 cm^{-1}) to inorganic (PO_4^{3-} at 960 cm^{-1}) contents (Figure 5b) within an area, illustrated the dominance of organic matter (Figure 5) in coronal cementum similar to root cementum. Structurally, although no fibrils in EDTA treated coronal cementum adjacent to enamel were observed (AAC in Figure 4), the presence of organic peaks between coronal cementum and enamel (shown by dashed lines in Figure 5b), could be due to variations in the density of reticular organic matter [23, 24]. Higher contents of noncollagenous organic matter within the reticular matrix could serve as a chemical adhesive resisting coronal cementum peel-off, which was also observed with some specimens. In contrast, if the ratio of organic to inorganic was lower in this region (shown by dashed lines in Figure 5b), it could encourage a peel-off under dry and high vacuum conditions as noticed in the SEM study (Figure 1b). However, there is no consensus if nonfibrillar matrix is derived from connective tissue (cementoblast, fibroblasts) or epithelium (ameloblasts and epithelial-sheath cells at the final stage of amelogenesis) [24].

AAC may be covered by acellular extrinsic fiber cementum and/or by junctional epithelium [22]. AEFC is located at cervical to mid-root portions where a high density of collagen fibers

insert, as seen from structure and chemical composition analysis in this study (Figures 4 and 5) [22]. Its organic matrix consists primarily of collagen with the typical banding pattern (Figure 5).

The structure and chemical composition of coronal cementums in other mammals such as equine and bovine, was described by intrinsic collagen running parallel to the CEJ with extrinsic collagen fiber bundles weaving obliquely through them [25]. However, equine and bovine teeth differ in CEJ microstructures. In bovine teeth it is smooth and flat, whereas it forms a micro-scallop integration with equine enamel, resulting in a greater toughness than that of bovine teeth [25]. In the case of humans it would be a challenge to estimate the interfacial toughness, because of the size limitation of coronal cementum and its natural tendency to flake (Figures 1-3), which could explain the fragility of this region and possible self-administered damage while maintaining recommended dental hygiene. It should also be noted that dry conditions during testing could encourage a differential shrinkage between coronal cementum, dentin and enamel that probably result in interfacial stresses and induces delamination at the weakest interface i.e. the coronal CEJ (Figure 1b) in comparison to the mechanically and chemically well-integrated dentin-enamel and cementum-dentin junctions.

The AEFC is produced by cementoblasts in close proximity to the advancing root edge during development. AEFC thus serves as the main anchorage of the tooth. Primary cementum predominantly consists of AEFC to which the gingival tissue could be attached under healthy conditions. Biomechanically, primary cementum attaches the tooth to the alveolar bone and partially accommodates masticatory forces, allowing optimum function. However, the function of the thin coronal cementum layer which is continuous with predominantly mineralized extrinsic fibrous primary cementum is not completely known. Theories include, guiding the tooth shape and tooth in its socket prior to root development [15]. However, in herbivorous mammals, from a biomechanics perspective, the softest and least wear resistant mineralized tissue i.e. coronal cementum on occlusal surface could accommodate different modes of masticatory forces [25,15].

Coronal cementum is heterogeneous with harder and softer regions

Site-specific estimation of elastic modulus and hardness provided results comparable to observed structure and chemical composition. Most often materials, including coronal cementum consisting of organic matrix, shrink, resulting in denser structures under dry conditions thus providing an over estimated modulus (15.7 ± 8.7 GPa) and hardness (1.3 ± 1.7 GPa) values [4,13]. However, the binding of water molecules to various hydrophilic constituents in the extracellular matrix of coronal cementum provides a less dense structure which is a closer approximation of physiological conditions. This results in lower elastic modulus (11.0 ± 5.8 GPa) and hardness (0.8 ± 1.3 GPa) values. The spread of data defines the heterogeneity of coronal cementum possibly due to varying structure and chemical compositions between AAC and AEFC. It should be noted that the observed hardness and reduced elastic modulus values of coronal and primary cementum of deciduous teeth are significantly higher than the reported values of secondary cementum taken from permanent human molars [8]. This could be due to the combinatorial effect of different contents of dietary and dental hygiene products including fluorine on the exposed coronal and primary cementum closer to the cervix. It should be noted that the higher values might reflect a combination of cementum and enamel modulus and hardness, which is inevitable due to the limited spatial sensitivity of the indenter.

5. CONCLUSIONS

The length of coronal cementum from the tooth cervix varies depending on the sectioning plane. This in turn suggests that a single tooth could exhibit all three types of cementum enamel

junctions. Coronal cementum is a combination of laminar AAC and fibrous AEFC with a relatively higher organic content making it into a heterogeneous material. It is continuous with primary root cementum apically and appears to integrate micromechanically via a weak interface with enamel unlike the DEJ and CDJ. Additionally, the elastic modulus of coronal cementum is significantly lower than primary cementum closer to the tooth cervix however, significantly higher than secondary root cementum.

Acknowledgments

This work was supported by the National Institute of Health and National Institute of Dental and Craniofacial Research (NIH/NIDCR) grants K99DE018212, R00DE018212, and P01 DE09859. The authors thank Gray Armitage, DDS and Mark Ryder, DMD, Division of Periodontology, Department of Orofacial Sciences, UCSF for many technical discussions. Additionally, the authors thank Lawrence Livermore National Laboratory for the use of Raman microspectrometer.

7. LITERATURE

1. Marshall SJ, Balooch M, Habelitz S, Balooch G, Gallagher R, Marshall GW. The dentin-enamel junction—a natural, multilevel interface. J Eur Ceram Soc 2003;23:2897–2904.
2. Lin CP, Douglas WH. Structure-property relations and crack resistance at the bovine dentin-enamel junction. J Dent Res 1994;73(5):1072–8. [PubMed: 8006234]
3. Zaslansky P, Friesem AA, Weiner S. Structure and mechanical properties of the soft zone separating bulk dentin and enamel in crowns of human teeth: insight into tooth function. J Struct Biol 2006;153 (2):188–99. [PubMed: 16414277]
4. Ho SP, Yu B, Yun W, Marshall GW, Ryder MI, Marshall SJ. Structure, chemical composition and mechanical properties of human and rat cementum and its interface with root dentin. Acta Biomater. 2008in print
5. Bevenius J, Lindskog S, Hultenby K. The Amelocemental junction in young premolar teeth. A replica study by scanning electron microscopy. Acta Odontol Scand 1993;51:135–42. [PubMed: 8342404]
6. Rose, LF.; Mealey, BL.; Genco, RJ.; Cohen, DW. Periodontics: medicine, surgery and implants. Elsevier Mosby; St.Louis: 2004.
7. Grzesik WJ, Narayanan AS. Cementum and periodontal wound healing and regeneration. Crit Rev Oral Biol Med 2002;13:474–84. [PubMed: 12499241]
8. Ho SP, Marshall SJ, Ryder MI, Marshall GW. The tooth attachment mechanism defined by structure, chemical composition and mechanical properties of collagen fibers in the periodontium. Biomaterials 2007;28(35):5238–45. [PubMed: 17870156]
9. Chutimanutskul W, Darendeliler MA, Swain MV, Shen G, Petocz P. Physical properties of human premolar cementum: hardness and elasticity. Aust Orthod J 2005;21(2):117–21. [PubMed: 16429867]
10. Alvarez-Pérez MA, Alvarez-Fregoso O, Ortiz-López J, Arzate H. X-ray microanalysis of human cementum. Microsc Microanal 2005;11(4):313–8. [PubMed: 16079015]
11. Schroeder HE, Listgarten MA. Fine Structure of the Developing Epithelial Attachment of Human Teeth. Monographs in Developmental Biology 1971;vol. 2
12. Brauer DS, Saeki K, Hilton JF, Marshall GW, Marshall SJ. Effect of sterilization by gamma radiation on nano-mechanical properties of teeth. Dental Materials 2008;24:1137–1140. [PubMed: 18436298]
13. Ho SP, Balooch M, Marshall SJ, Marshall GW. Local properties of a functionally graded interphase between cementum and dentin. J Biomed Mater Res A 2004;70(3):480–9. [PubMed: 15293322]
14. Pharr GM, Oliver WC, Brotzen FR. On the generality of the relationship among contact stiffness, contact area, and elastic modulus during indentation. J. Mater. Res 1992;7:613–617.1992
15. Boyde A. Understanding the structure of the mammalian mineralized tissues through their development. Mater. Res., Soc., Symp., Proc 2006:898 E.
16. Wang R, Hu Y, Ng C. Microstructure and interfacial fracture at the cementum-enamel junctions in equine and bovine teeth. J. Mater. Res 2006;21(8)
17. Kozawa Y, Chisaka H, Iwasa Y, Yokota R, Suzuki K, Yamamoto H. Origin and evolution of cementum as tooth attachment complex. J. Oral. Biosci 2005;47(1):25–32.

18. Listgarten MA. A light and electron microscopic study of coronal cementum. Arch Oral Biol 1968;13:93–114. [PubMed: 5237558]

19. Schroeder, HE.; Listgarten, MA. Monographs in Developmental Biology. Vol. 2nd Ed. S. Krager AG; 1977. Fine structure of the developing epithelial attachment of human teeth; p. 42

20. Jones SJ, Boyde A. Coronal cementogenesis in the horse. Arch Oral Biol 1974;19(8):605–14. [PubMed: 4532487]

21. Hassel TM. Tissues and cells of the periodontium. Periodontol 2000 1993;3:9–38. [PubMed: 9673156]

22. Bosshardt DD, Selvig KA. Dental Cementum: the dynamic tissue covering of the root. Periodontol 2000 1997;13:41–75. [PubMed: 9567923](1997)

23. Schroeder, HE.; Listgarten, MA. Monographs in Developmental Biology. Vol. 2nd Ed. S. Krager AG; 1977. Fine structure of the developing epithelial attachment of human teeth; p. 38

24. Kodaka T, Debari K. Scanning electron microscopy and energy-dispersive X-ray microanalysis studies of afibrillar cementum and cementicle-like structures in human teeth. J Electron Microsc 2002;51(5):327–35.

25. Wang R, Hu Y, Ng C. Microstructure and interfacial fracture at the cementum-enamel junctions in equine and bovine teeth. J. Mater. Res 2006;21(8)

26. Nanoscope® Command Reference Manual. Digital Instruments Inc.; 1998. p. 1-22-1-25.

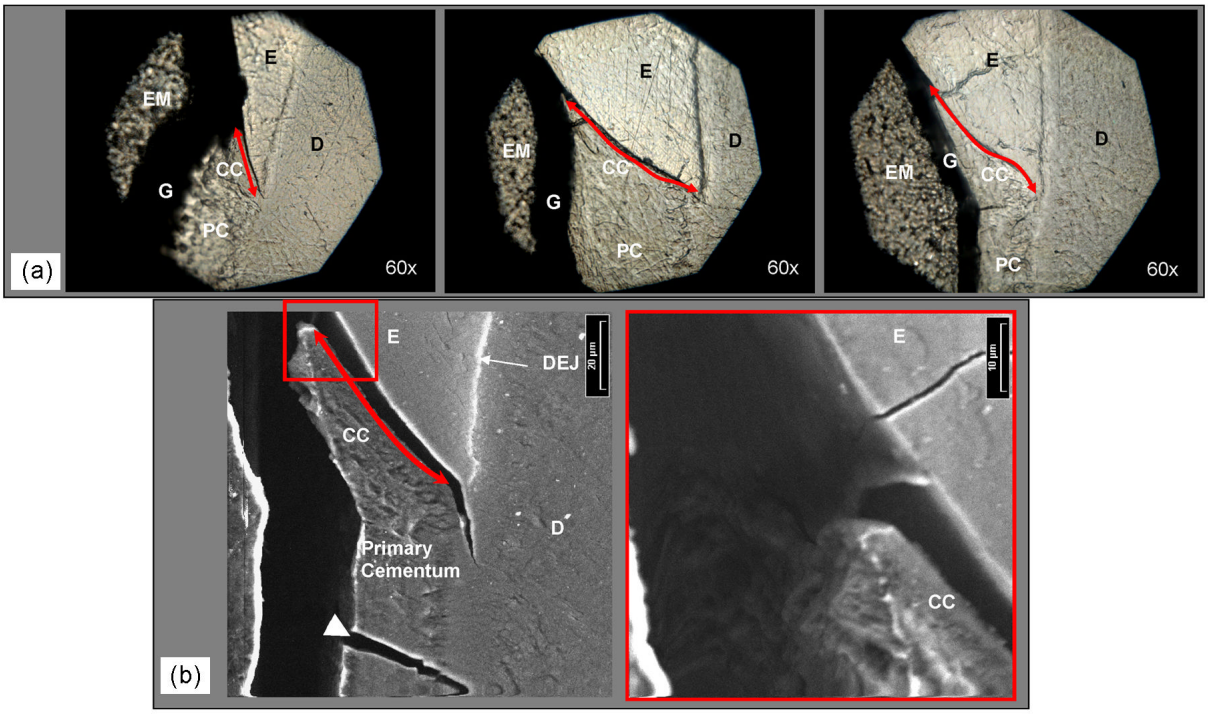

FIGURE 1.

a). Light microscopy micrographs of polished specimens taken at 60X magnification. The solid red-line defines the overlap region of cementum with enamel termed as coronal cementum. The octagonal shape encompassing the specimen is the aperture of the light microscope. The aperture was partially closed to create contrast and better visualization of the specimen. **b**). Scanning electron micrographs illustrate peeling-off of coronal cementum (curved double ended red arrow) from enamel at lower (black scale bar 20 μm) and higher magnifications (black scale bar 10 μm). Note: EM-Embedding Material; G – a finite gap between embedding material and specimen; CC – Coronal Cementum; PC – Primary Cementum; E – Enamel; D – Dentin.

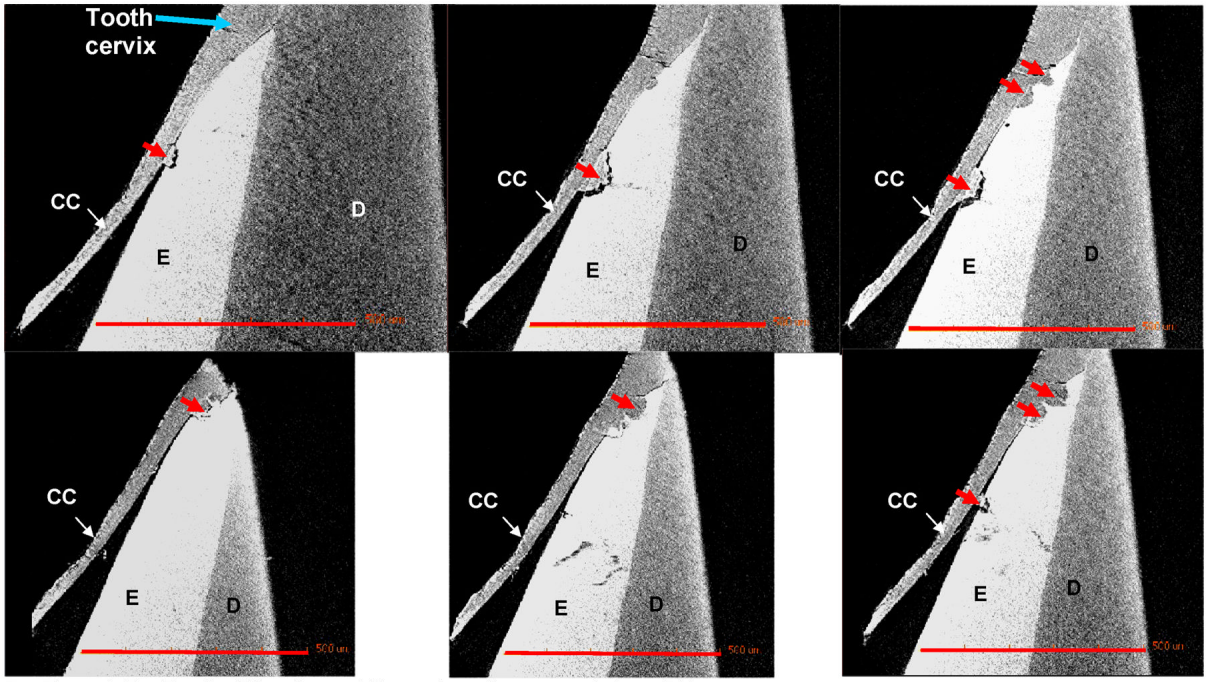

E – Enamel; D – Dentin; CC – Coronal Cementum; Orange scale bar: 500 μm

FIGURE 2.

MicroXCT™ 2D reconstructed slices illustrating scalloped appearance; scallop-like integration of mid-CC and proximal-CC with enamel (the location of mid-CC and proximal-CC are with respect to the tooth cervix). Notice that integration of CC with enamel (red arrows) varies through the specimen thickness. Additionally, notice that mid-CC is poorly adherent to enamel in comparison to proximal-CC.

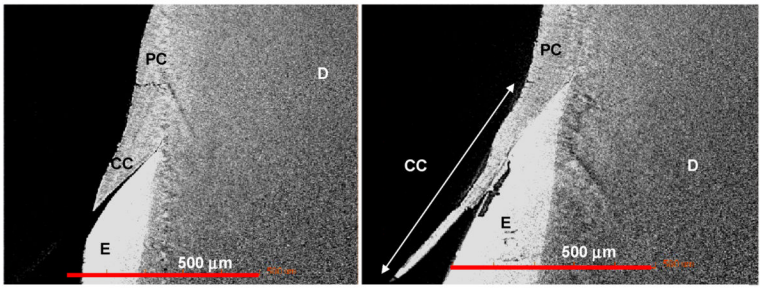

E – Enamel; D – Dentin; CC – Coronal Cementum; PC – Primary Cementum; Orange scale bar: 500 µm

FIGURE 3.

MicroXCT™ 2D reconstructed slices illustrating the variation in length of (coronal cementum) CC as a function of specimen thickness.

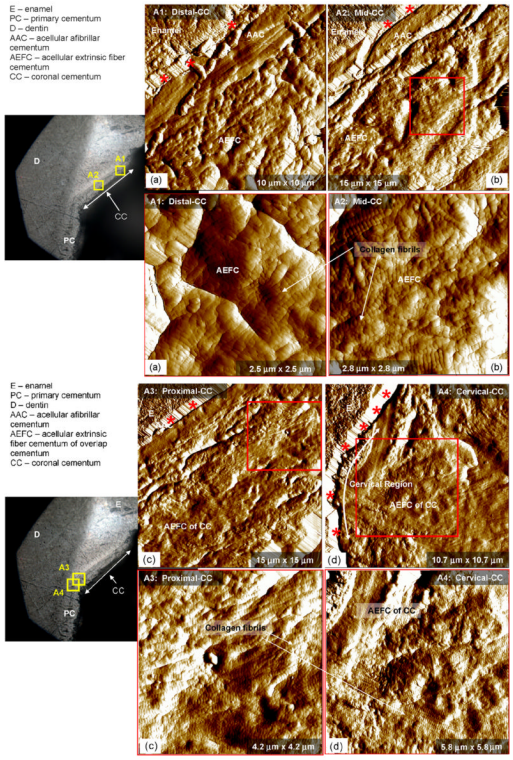

FIGURE 4.

High resolution atomic force micrographs of 10 min EDTA treated specimens identifying acellular extrinsic fiber cementum (AEFC) and acellular afibrillar cementum (AAC) within distal-CC (**4a**), mid-CC (**4b**), proximal-CC (**4c**), and cervical-CC (**4d**). The dark lines seen in corresponding light microscope images are valleys as seen using an AFM. Note: Most often specimen preparation induces a valley-like artifact between two dissimilar materials such as cementum and enamel. However, the topography of the valley-walls (red askerisks) is an artifact of imaging caused due to specimen-surface and tip-geometry limitations [8,26].

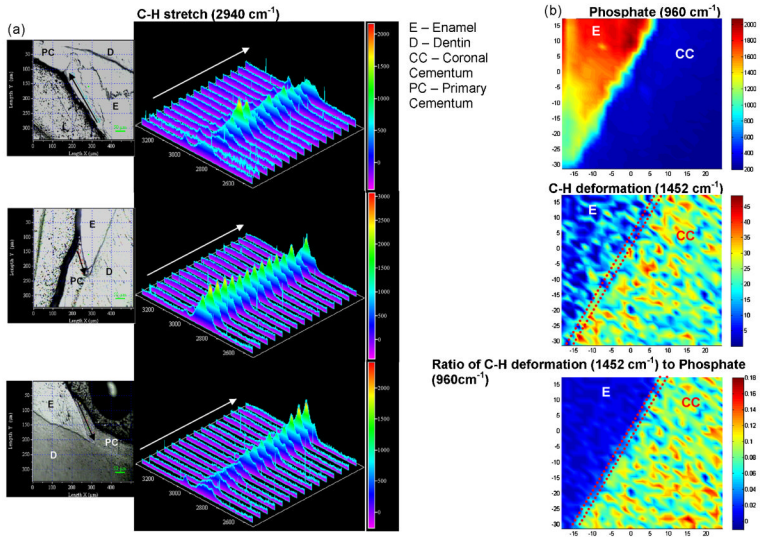

FIGURE 5.

a). Raman microspectroscopy of three specimens, illustrating the presence of organic matter (C-H stretch at 2940 cm^{-1}) along the length of coronal cementum shown by the black and white arrows in respective images. **b**). Area map illustrates the spatial variation of phosphate (960 cm^{-1}), C-H deformation (1452 cm^{-1}), and ratio of C-H deformation (1452 cm^{-1}) to phosphate (960 cm^{-1}). Note the presence of organic peaks within the dashed lines illustrating the presence of organic matter between enamel and coronal cementum.

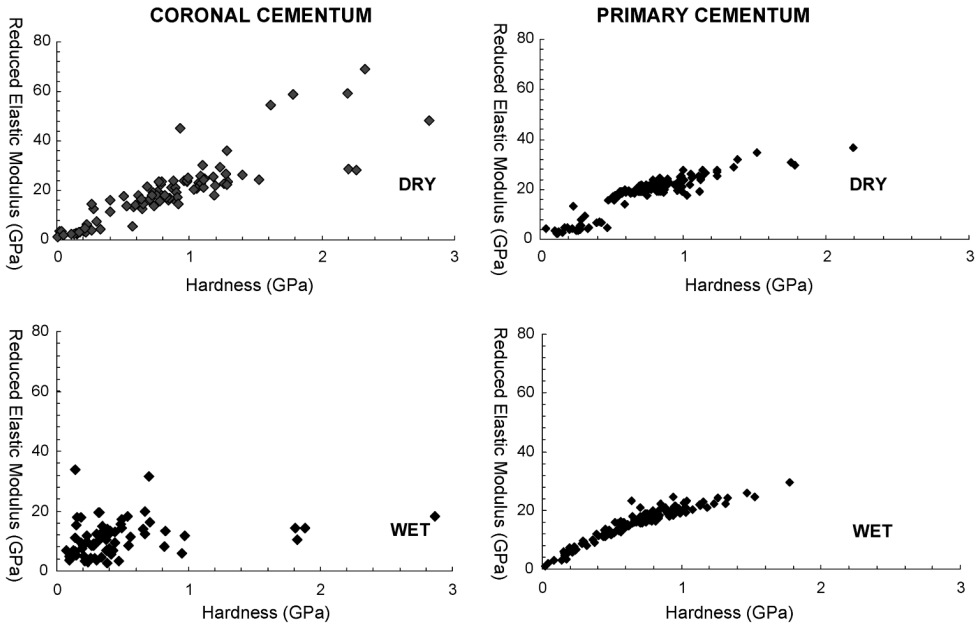

FIGURE 6.

The spread of elastic modulus vs. hardness for primary cementum (PC) and coronal cementum (CC) under dry and wet conditions.